IOP Conf. Series: Materials Science and Engineering **278** (2017) 012083 doi:10.1088/1757-899X/278/1/012083

Liquid helium free cryogenic mechanical property test system with optical windows

H C Zhang[1,2], C J Huang[1], R J Huang[1,2] and L F Li[1,2]

[1]State Key Laboratory of Technologies in Space Cryogenic Propellants, Technical Institute of Physics and Chemistry, Chinese Academy of Sciences, Beijing 100190, PR China
[2]University of Chinese Academy of Sciences, Beijing 100049, China
E-mail: laifengli@mail.ipc.ac.cn

Abstract. Digital image correlation (DIC) is a non-contact optical method for the in-plane displacement and strain measurement, which has been widely accepted and applied in mechanical property analysis owing to its simple experimental steps, high accuracy and large range of measurement. However, it has been rarely used in cryogenic mechanical test since the opaque design of cryostats and the interaction of optics with liquid coolants (liquid nitrogen or liquid helium). In the present work, a liquid helium free cryogenic mechanical property test system cooled by G-M cryocoolers, with a continuous, tunable environmental temperature from room temperature down to around 20 K, was developed and tested. Quartz optical windows, which are compatible with 2D DIC technology, were designed and manufactured on both inner and outer vacuum chambers. The cryogenic test system with optical windows satisfies well for mechanical tests of materials and takes advantage of both being compatible with DIC technology and getting rid of the use of expensive liquid helium. Surface displacement and strain field of Ti6Al4V under uniaxial tension were studied at 20 K by using this system. The results obtained by DIC method agree well with those obtained by extensometers at cryogenic temperatures.

Keywords: G-M cryocooler; cryogenic mechanical property; DIC; optical windows

1. Introduction

Mechanical properties such as strength, toughness and ductility of materials at low temperatures play a crucial role in design of various components operating below ambient temperature. In general, these mechanical properties can be measured through laboratory measurement to imitate real service [1-4]. To investigate mechanical properties at low temperatures, surface deformation behaviours at both macro- and micro-scales subjected to mechanical loadings are of great importance. Aside from widely used pointwise strain gauge technique, various full-field non-contact optical methods have been developed and applied for this purpose [5-7].

Digital image correlation (DIC) is a non-contact optical method for surface elastic, plastic deformation and fracture measurement, which has been widely accepted and applied in mechanical property test because of its incomparable advantages such as the simple experimental steps, high accuracy and large range of measurement. A number of researches have demonstrated that this technique is easily to manipulate and can provide satisfactory resolution of displacement and strain fields [8-11]. Moreover, the DIC technology can acquire localized properties across small scale like

thin weld region where traditional extensometer fails. However, the DIC technique has been rarely used in cryogenic mechanical tests so far. This is because the current opaque cryostats used for mechanical tests can't allow for passing through of light beam. Moreover, the interaction of light with liquids as well as small bubbles on the surface of specimen resulting from adiabatic deformation inevitably distort the image although the light can penetrate the transparent coolants.

In this work, a cryogenic mechanical property test system with optical windows cooled by G-M cryocoolers was developed. The quartz optical windows which allow for two separated light paths are compatible with the DIC technology. Furthermore, the cryogenic mechanical test system is independent of expensive liquid helium. Elastic modulus and Poisson ratio of Ti6Al4Vwere measured at 20 K by using this system and the results were compared with those obtained through cryogenic-grade extensometers.

2. Experimental Details

The system mainly consists of cryogenic chambers with optical windows, cooling and temperature control system, mechanical frame, testing machine and DIC components. Figure 1(a) shows the schematic of the cryogenic mechanical property test system and a photograph of the experimental setup is shown in figure 1(b) with unfiltered white light illumination and a zoomed camera showing the placement of the sample in the sample chamber.

The cryogenic chambers with optical windows provide cryogenic environment for the test specimen and the light paths for incident light and camera. The cooling and temperature control system consists of two G-M cryocoolers which cool the cryogenic environment down to cryogenic temperature and a heater and controller to heat the cryogenic environment to interesting temperature, which connect directly to the sample chambers. During the cooling process, the sample chamber was cooled by two G-M cryocoolers and helium gas was filled into the chamber to speed up the heat exchange which would convey the heat from mechanical support frame and sample to sample chamber. The heat exchange between the test sample and sample chamber is mainly dependent on helium gas convection.

The mechanical frame, which connects to the testing machine and installs into the sample chambers, transfers the pulling load from the test machine at room temperature to the test specimen at low temperatures. The specimen chambers and the mechanical frame can be easily installed to a static or fatigue testing machine. In the present work, a fatigue machine (model: SUNS PLS 100) equipped with cryogenic-grade extensometers and the 2D DIC were both used. The DIC can directly provide full-field displacements to sub-pixel accuracy and full-field strains by comparing the digital images of a test object surface acquired before and after deformation through optical windows.

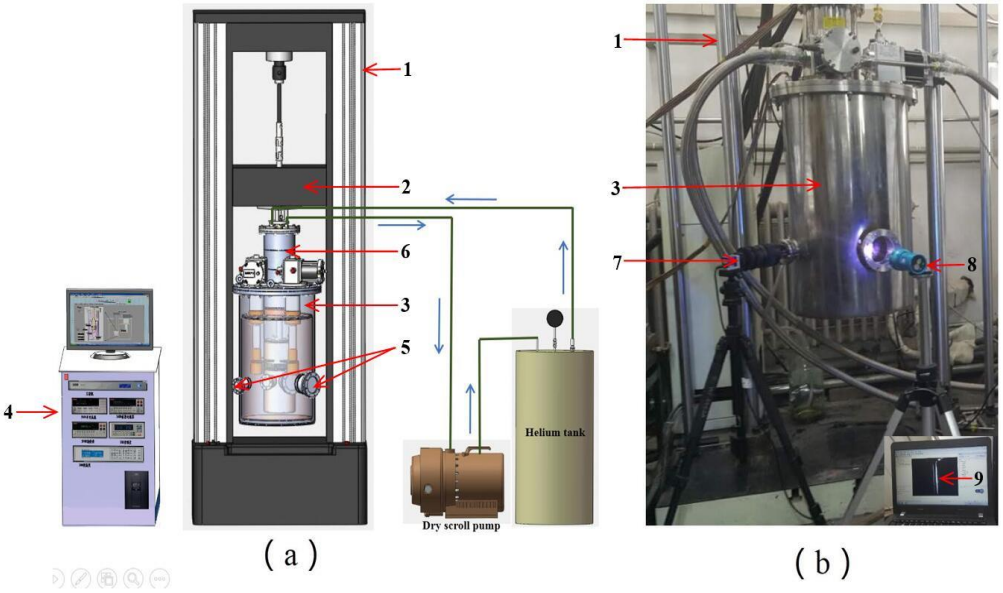

(a) (b)

Figure 1. (a) Scheme of the cryogenic mechanical property testing system, and (b) Photo of experimental setup: (1) mechanical testing machine, (2) cross-beam, (3) cooling system, (4) data control system, (5) optical windows, (6) sample chamber, (7) camera with zoom lenses and CCD, (8) unfiltered white light source, (9) zoomed sample.

2.1. Cryogenic system and optical windows

The cryogenic chambers fall into two parts, the outer vacuum chamber and the inner specimen chamber. Figure 2 shows the detail of the cryogenic chambers with optical windows. The outer vacuum vessel is made of 304 stainless steel with an external diameter and a height of 450 mm and 720 mm, respectively, which was pumped to a pressure less than 10^{-3} Pa and provided a vacuum environment for the inner sample chamber.

The two cold heads of the G-M cryocooler was installed and sealed into the outer vacuum chamber. The thermal radiation shield with multilayer insulation material (MLI) was installed in the inner sample chamber. The sample chamber, made up of two parts, was installed in the vacuum vessel. The bottom which is made of oxygen-free high conductivity copper (OFHC) is used for thermal conduction and contacted with second-stage cold heads of G-M cryocoolers through thermal bridges. Thermal bridges are also made of OFHC. The upper part is applied to thermal insulation thus it was low thermal conductivity 304 stainless steel and contacted with first-stage cold heads of G-M cryocoolers through copper radiation shield flange. To decrease contact thermal resistance, Apiezon N and indium were used between the flange and the radiation shield, and between the joints. Moreover, a helium gas container with valve was connected to the sample chamber.

Four optical windows were designed on both the outer vacuum vessel and the sample chamber, which allows for two separately light paths. The optical windows of one light path with a diameter of 100 mm were devoted to make the emitted light to adequately illuminate the sample surface. The optical windows of another light path with a diameter of 60 mm were applied to take high resolution digital images before and after deformation by using a high-contrast speckle pattern of the object's surface by the DIC technique.

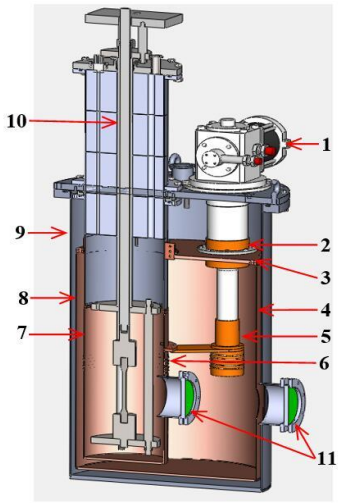

Figure 2. Construction details of the cooling system: (1) cryocooler, (2) first-stage cold head, (3) copper flange, (4) thermal bridge, (5) second-stage cold head, (6) heater, (7) sample chamber, (8) radiation shield, (9) vacuum vessel, (10) pulling rod, (11) optical window.

All optical windows consist of two 304 stainless steel flanges and one quartz glass. The sealing method of quartz glass was distinct in different positions. The optical windows, mounted on sample chamber, were sealed with indium and polytetrafluoroethylene gaskets. Indium was used between inner flange and quartz glass then they were irresistibly attached. Polytetrafluoroethylene gasket, as the middle medium, was used between outer flange and quartz glass. It can avoid the damage of quart glass. Moreover, the optical windows, installed on vacuum vessel, were hermetically sealed with O-

ring. Flanges have one O-ring groove respectively, which can avoid O-ring slipping and make flanges contact closely with quartz glass.

Several thermometers were separately mounted at copper sample chamber, second stage cold head, thermal radiation shield and sample to obtain localized temperatures.

2.2. Mechanical frame

The tensile testing mechanical design mainly consists of a mechanical frame with accessories including insulation foam with low cryogenic thermal conductivity, thermometer binding post used in vacuum vessel and copper sheet applied to radiation shielding. The main configuration of the mechanical frame is shown in figure 3.

The pulling rode (4) is made of an annealed Ti6Al4V alloy, because it has high mechanical strength at both room and cryogenic temperatures as well as low cryogenic thermal conductivity [12,13]. All other components (1-3, 5-9) except accessories are made of 304 austenitic stainless steel due to its relative high strength, ductility at cryogenic temperatures, and low cryogenic thermal conductivity [14,15].

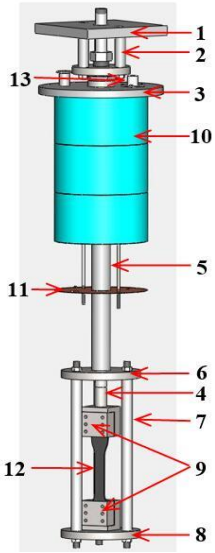

Figure 3. Configuration of mechanical frame: (1) connection plate, (2) four supporting rods, (3) flange, (4) pulling rod, (5) supporting tube, (6) top mounting plate, (7) three supporting rods, (8) down mounting plate, (9) testing jigs, (10) insulation material, (11) copper sheet, (12) sample, (13) binding post.

The connection plate (1) can be directly installed and fixed to a cross head of the static or fatigue testing machine. The four supporting rods (2) joint the connection plate (1) and the flange (3). The flange (3) is applied to seal the sample chamber which has one O-ring groove. The supporting tube (5) with an inner and outer diameter of 23 mm and 35 mm respectively connects the flange (3) with the top mounting plate (6). The supporting tube (5) joints the flange (3) by welding. Moreover, the joint between supporting tube (5) and the top mounting plate (6) is threaded connection. The top mounting plate (6) and the bottom supporting plate (8) are connected by the three supporting rods with length of 330 mm in an equilateral triangle orientation. The top mounting flange has a centre through hole which contributes the pass of the pulling rode (4). The top and bottom test jigs, which can be easily fixed and removed, connect the specimen to the pulling rod (4) or the down mounting plate (8). Moreover, the test jigs (9) have various configurations to perform tension tests of plate or round bar specimen, fracture toughness tests, and tension-tension fatigue tests.

The length of the three supporting rods (7) is 330 mm. This distance is used for the top and bottom test jigs, the test sample as well as space for extension of sample. For tension tests, the length of the sample is usually less than 250 mm (ASTM Standard E8, ASTM Standard E1450, ASTM

Standard D638, ASTM Standard D3039 approved), thus the distance is enough for both non-metallic and metallic materials with high ductility.

2.3 Elastic modulus and Poisson's ratio of Ti6Al4V

The elastic modulus and Poisson's ratio of Ti6Al4V were investigated at 20 K by using this system. As a comparison, the elastic modulus and Poisson's ratio were simultaneously calculated by using cryogenic-grade extensometers. During the test, the loads were slowly applied to 1, 2, 3, 4, and 5 kN with a cross-beam velocity of 0.2 mm/min. The patterns obtained through the DIC technology, the axial and transverse strains obtained through two separately extensometers were recorded at different loads.

3. Results and Discussion

3.1. Cooling procedure

The sample chamber is purified and charged with 99.999% helium gas. The vacuum vessel is vacuumed up to 10^{-3} Pa before the cryocoolers are turned on. Figure 4 shows the cooling progress of the test system.

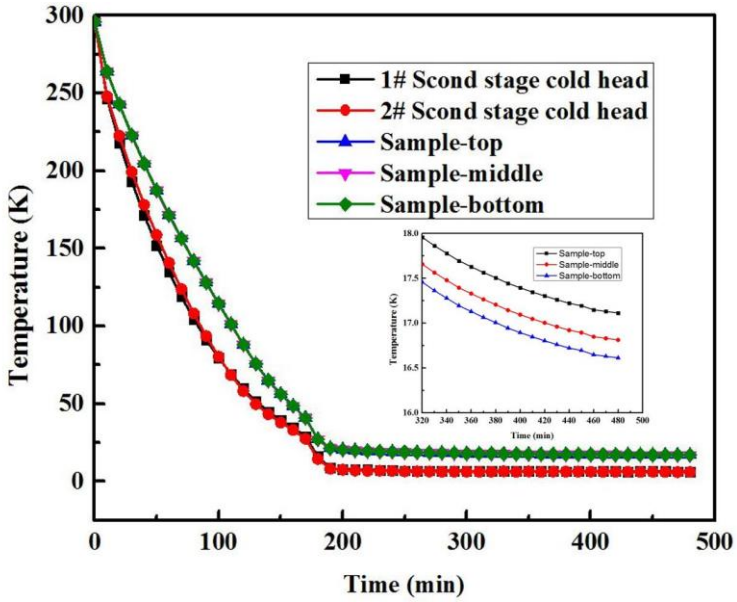

Figure 4. Temperature of testing system changing with time during the system cooled

From figure 4, we can see that it takes around 8 hours to make the temperature of sample cool down to 16.8 K. In the beginning, the sample temperature drops quickly with a high cooling rate. With the reduction of temperature, the sample cooling rate decreases for the decline of the temperature difference between second stage cold head and sample. Cooling curve begins to smooth at the time of 3 h. At this time, second stage cold head temperatures are about respectively 8.5 K and 8.1 K and sample temperature is approximately 21.2 K. At the cooling time of 8 h, sample temperature drops to 16.8 K and the cooling rate of sample becomes very small. The temperature difference between second stage cold head and sample is about 10 K and the cooling system achieves thermal equilibrium. The maximum temperature difference of sample at different position is about 0.3 K. As the expected temperature is steady, testing machine is turned on and mechanical performance tests will be performed.

3.2. Experimental results from the analysis of the displacements field using DIC

Tensile sample of titanium alloy was cooled by using this cryogenic system and observed under unfiltered light. Surface displacement and strain field of titanium alloy were then computed under different loads by making use of DIC at 20 K. Experiment was performed by using laminar tensile

sample with square gauge region. A schematic and photograph of the machined sample is provided in figure 5. The cross-section of sample is considered to a 15×3 mm square cross-section.

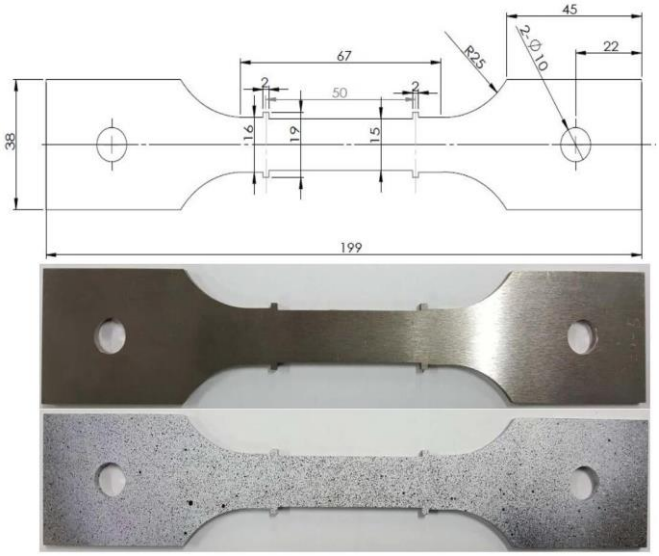

Figure 5. Schematic of gauge region test sample (above) and photo of sample with unspeckled gauge region (middle) and speckled gauge region (bottom)

The speckle pattern was applied to one side of square gauge region in order to compute the relative displacements of the speckled surface by a computer algorithm. This sample was subjected to uniaxial tension under displacement control in a servohydraulic load machine. The sample was loaded at a rate of 0.2 mm/min and the image of the speckled surface was recorded when the load was added per 1 kN. The camera was capable of detecting both visible and light with a resolution of 2592×1944 pixels. The taken images of gauge region were approximately 753×1939 pixels, and the correlation was performed by using 41×41 pixel subsets with a step size of 10 pixels. Before loading tension, the sample was cooled to the desired temperature (20 K) without load. The image of this moment was also recorded. The surface of sample at various loads in unfiltered white light is shown in figure 6 (a).

It is evidenced the gradual shifting of the grayscale distribution towards higher grayscale values due to the increasing of load. Displacement fields of sample undergoing such loads are given in figure 6 (b). These results are from a correlation between an unloaded image state and loaded images. Figure 6 (b) shows that the horizontal average displacement decreases with load increasing, which is consistent with Poisson's ratio under uniaxial tension. Moreover, the vertical average displacement increases with load increasing, which is also consistent with uniaxial tension. The results of strain at different loads, Young's modulus and Poisson's ratio are compared between applying DIC technique and using Epsilon extensometers, which is shown in table 1. The average of the Young's modulus and the Poisson's ratio obtained by the DIC technology and the extensometers related to different load values are reported. It is shown that the obtained results from DIC technique have slight deviation compared with extensometer.

Table 1. Results compared using different test methods

Method	Strain (1kN)	Strain (2 kN)	Strain (3kN)	Strain (4kN)	Strain (5kN)	Young's modulus (GPa)	Poisson's ratio
DIC	0.016%	0.032%	0.047%	0.063%	0.082%	139	0.33
Extensometer	0.021%	0.041%	0.058%	0.079%	0.101%	110	0.30

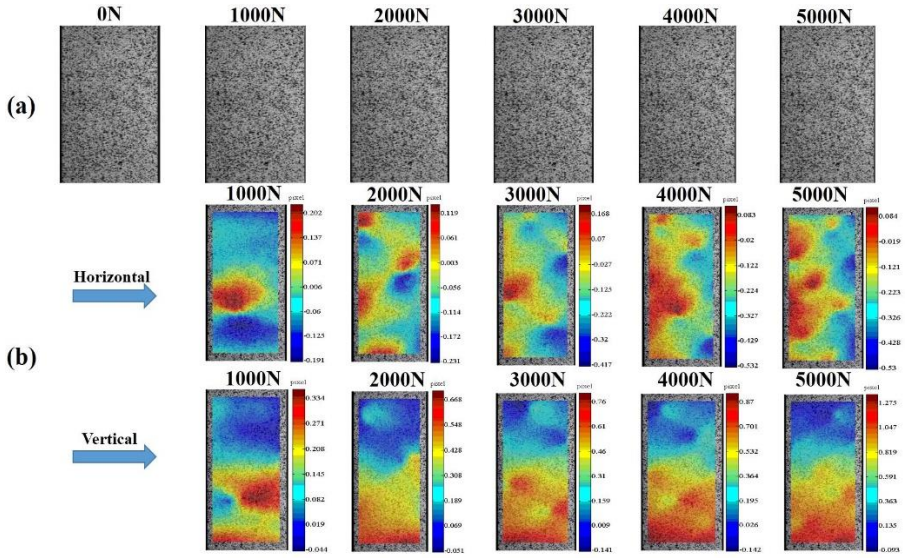

Figure 6. (a) Images of the speckled surface at different loads, (b) Contours of horizontal and vertical displacement (in pixels) at different loads.

4. Conclusions

In this work, a liquid helium free cryogenic mechanical property test system with optical windows for DIC technology was designed and tested. The system can provide a continuous, tunable environmental temperature from room temperature down to around 20 K. The surface displacement and strain field of Ti6Al4V under uniaxial tension were studied at 20 K by using this system. The results indicate that the cryogenic test system with optical windows can satisfy well for DIC analysis on mechanical property tests. The system will be extended to investigate thermal contraction of materials as well as strain fields of crack tip at low temperatures in the future.

References

[1] T. Ogata and K. Ishikawa, A new liquid-helium temperature fatigue testing system. *Transactions of the Iron and Steel Institute of Japan*, 1986. **26**(1): p. 48-52.

[2] A. Nishimura, Need for development of higher strength cryogenic structural materials for fusion magnet. *Advances in Cryogenic Engineering*, Vol 60, 2014. **1574**: p. 333-339.

[3] C. Compton, S.K. Chandrasekaran, D. T. Baars, Bieler, P. Darbandi, N. Wright, Development of a cryogenic mechanical property testing station for superconducting RF cavity material. *Advances in Cryogenic Engineering*, Vols 55a and 55b, 2010. **1218**: p. 587-594.

[4] W.L. Johnson, R.C. Youngquist, T.L. Gibson, S.T. Jolley, M.K. Williams, Measurement of the mechanical properties of thin film polymers at cryogenic temperatures. *Advances in Cryogenic Engineering*, Vol 60, 2014. **1574**: p. 162-169.

[5] B. Pan, K.M. Qian, H.M. Xie, A. Asundi, Two-dimensional digital image correlation for in-plane displacement and strain measurement: a review. *Measurement Science and Technology*, 2009. **20**(6): p. 2001-2017.

[6] Z.B. Zhou, P.W. Chen, and F.L. Huang, Study on dynamic fracture and mechanical properties of a Pbx simulant by using DIC and Shpb method. *Shock Compression of Condensed Matter - 2011*, Pts 1 and 2, 2012. **1426**: p.665-668.

[7] P. Lopez-Crespo, M. Mostafavi, A. Steuwer, J.F. Kelleher, T. Buslaps, P.J. Withers, Characterisation of overloads in fatigue by 2D strain mapping at the surface and in the bulk. *Fatigue & Fracture of Engineering Materials & Structures*, 2016. **39**(8): p. 1040-1048.

[8] R.B. Berke, and J. Lambros, Ultraviolet digital image correlation (UV-DIC) for high temperature applications. *Review of Scientific Instruments*, 2014. **85**(4): p.045121-1-9.

[9] J.M. Vasco-Olmo, F.A. Diaz, A. Garcia-Collado, R. Dorado-Vicente, Experimental evaluation of crack shielding during fatigue crack growth using digital image correlation. *Fatigue &*

Fracture of Engineering Materials & Structures, 2015. **38**(2): p. 223-237.
[10] R. Wu, C. Kong, K. Li, D. Zhang, Real-time digital image correlation for dynamic strain measurement. *Experimental Mechanics*, 2016. **56**(5): p. 833-843.
[11] W. Wang, C.H. Xu, H. Jin, S.H. Meng, Y.M. Zhang, W.H. Xie, Measurement of high temperature full-field strain up to 2000 degrees C using digital image correlation. *Measurement Science and Technology*, 2017. **28**(35): p. 7-13.
[12] V. Martelli, and G. Ventura, Low temperature thermal conductivity of candidate materials for the supports of CUORE. *Low Temperature Detectors Ltd 13*, 2009. **1185**: p. 685-688.
[13] T. Yuri, Y. Ono, T. Ogata, H. Sunakawa, Effect of microstructure on high-cycle fatigue properties of Ti-6Al-4V alloy forging at cryogenic temperatures. *Advances in Cryogenic Engineering*, Vol 60, 2014. **1574**: p. 27-33.
[14] W. Stutius, and J.R. Dillinger, Magnetic and thermal properties of some austenitic stainless-steels at low-temperatures. *Journal of Applied Physics*, 1973. **44**(6): p. 2887-2888.
[15] T. Ogata, Hydrogen embrittlement evaluation in tensile properties of stainless steels at cryogenic temperatures. *Advances in Cryogenic Engineering*, Vol 54: Transactions of the International Cryogenic Materials Conference - ICMC, 2008. **986**: p. 124-131.

Acknowledgements
This work was supported by the National Natural Science Foundation of China (Grant No. 51427806, 51401224, 51577185, 51406217), the Foundation of CAS (Grant No. QYZDB-SSW-JSC042) and the fund of the State Key Laboratory of Technologies in Space Cryogenic Propellants, SKLTSCP1504, SKLTSCP1701 and the National Magnetic Confinement Fusion Science Program (Grant No. 2015GB 121001). The authors would like to thank Prof. A. Nishimura and Prof. T. Ogata for valuable suggestions.